An Ice-Motion Tracking System at the Alaska SAR Facility

RONALD KWOK, MEMBER, IEEE, JOHN C. CURLANDER, ROSS McCONNELL, AND SHIRLEY S. PANG

Abstract—**An operational system for extracting ice-motion information from Synthetic Aperture Radar (SAR) imagery is being developed for installation at the University of Alaska, Fairbanks, as part of the Alaska SAR Facility. This Geophysical Processing System (GPS) will derive ice-motion information by automated analysis of image sequences acquired by radars on the European ERS-1, Japanese ERS-1, and Canadian RADARSAT remote sensing satellites. The algorithm consists of a novel combination of feature-based and area-based techniques for the tracking of ice floes that undergo translation and rotation between imaging passes. The algorithm development was motivated by the requirement for a highly reliable and efficient operational system for routine production of a regular gridded matrix of ice-motion vectors. Additional complexity in image segmentation is added by the unique characteristics of the SAR data, such as speckle noise, large dynamic range, and radiometric distortions. The system performs automatic selection of the image pairs for input to the matching routines using an ice-motion estimator. The system is designed to have a daily throughput of ten image pairs. This paper describes the GPS system, including an overview of the ice motion tracking algorithm, the system architecture, and the ice-motion products which will be available for distribution to geophysical data users.**

I. INTRODUCTION

THE ALASKA SAR Facility (ASF), to be located in Fairbanks, Alaska, will receive, record, process, and disseminate SAR data acquired by the European ERS-1, Japanese ERS-1, and Canadian RADARSAT satellites. The Alaska SAR Facility (ASF) will be the first fully integrated system for handling large volumes of SAR data ever built by NASA. A block diagram of the facility is shown in Fig. 1. It consists of three subsystems: 1) The receiving ground station; 2) the high-speed SAR processor; and 3) an archive and operations system that supports a geophysical processor and an image analysis workstation. The science objectives of the ASF program are multidisciplinary, including studies in air–sea–ice interaction, oceanography, glaciology, geology, hydrology, and ecology. To support these studies, a Geophysical Processor System (GPS) is being developed to enable manipulation and analysis of the ASF data as well as routine generation of geophysical products. Presently, the GPS has two components: An Ice/Oceans Processor, and an image anaysis workstation. This paper focuses on only one of the functions of the Ice Processor GPS, the generation of ice motion products from time-sequential SAR images. The products include sea-ice kinematic data sampled on a pre-defined spatial and temporal grid, with embedded meteorological data acquired from national weather centers. Other GPS products such as the ice classification and ocean wave characteristics will be discussed in a future paper.

Ice motion is of interest in a number of contexts [1]; namely, latent heat advection, oceanic surface stress, passive tracing of currents, open water production by way of ice divergence and shear, and interaction between icebreaker navigation and ice structure. Within the central ice pack, the complex nature of the relative motion under divergence and shear remains a research area. The relative motion creates both open water through which significant heat is lost, and ridges which contain a large fraction of the total sea-ice volume and are operational hazards. At the margin, the thermal processes associated with opening and closing are also significant; this is particularly the case at coastal margins where ice formation results in the production of cold brine which flows down the continental shelf to mix and sink to the bottom or an intermediate depth. In addition to aiding the understanding of the physical processes, the applications of monitoring the state of polar sea ice include operational forecasting of weather and ice conditions, evaluation of natural hazards, and the environmental impacts of Arctic development.

The utilization of SAR data for the analysis of sea-ice motion has been described in several papers [1]–[4]. These techniques are dependent on time-consuming visual identification of corresponding ice features in sequential image frames which have been radiometrically and geometrically corrected. For the large volume of data which will be collected by operational SAR systems, the aforementioned supervised techniques for extensive motion analysis are impractical, thus necessitating the development of automated techniques. A number of automated techniques for construction of ice motion data using SAR images has been suggested by [5]–[8]. All of these techniques, which are essentially based on area correlation for matching corresponding image patches, are limited by the fact that area correlation can measure only spatial lags. The correlation peak broadens and eventally becomes statistically insignificant as the ice motion rotational component becomes large. One approach [7] did consider tracking the rotation of ice features using floe-lead boundaries; however, the utility was demonstrated only on image features with small rotations.

Manuscript received April 26, 1989; revised September 25, 1989. This work was supported by the National Aeronautics and Space Administration.

R. Kwok, J. C. Curlander, and S. S. Pang are with the Jet Propulsion Laboratory, California Institute of Technology, 4800 Oak Grove Drive, Pasadena, CA 91109.

R. McConnell is with the Vexcel Corporation, 2477 55th Street, Boulder, CO 80301.

IEEE Log Number 8932244.

0364-9059/90/0100-0044 $01.00

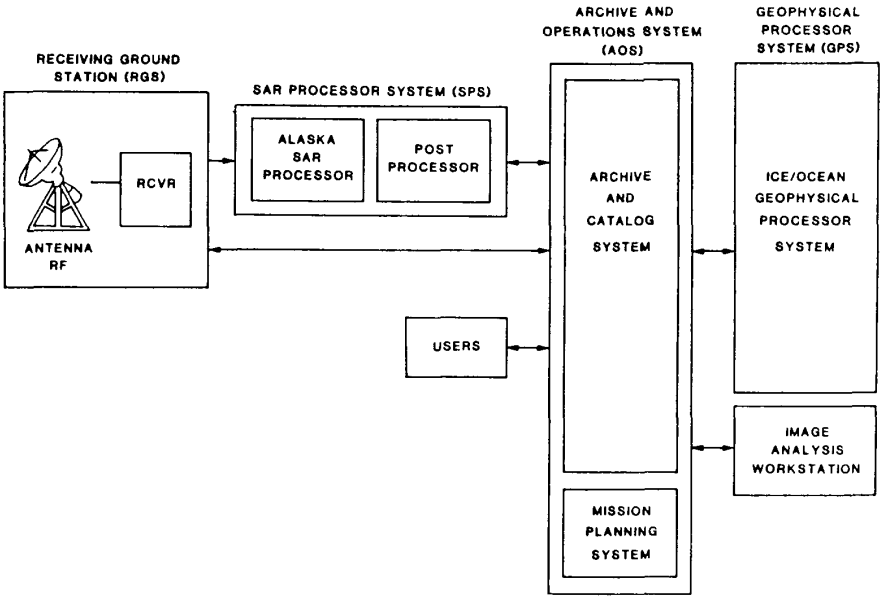

Fig. 1. Block diagram showing the three subsystems of the Alaska SAR facility.

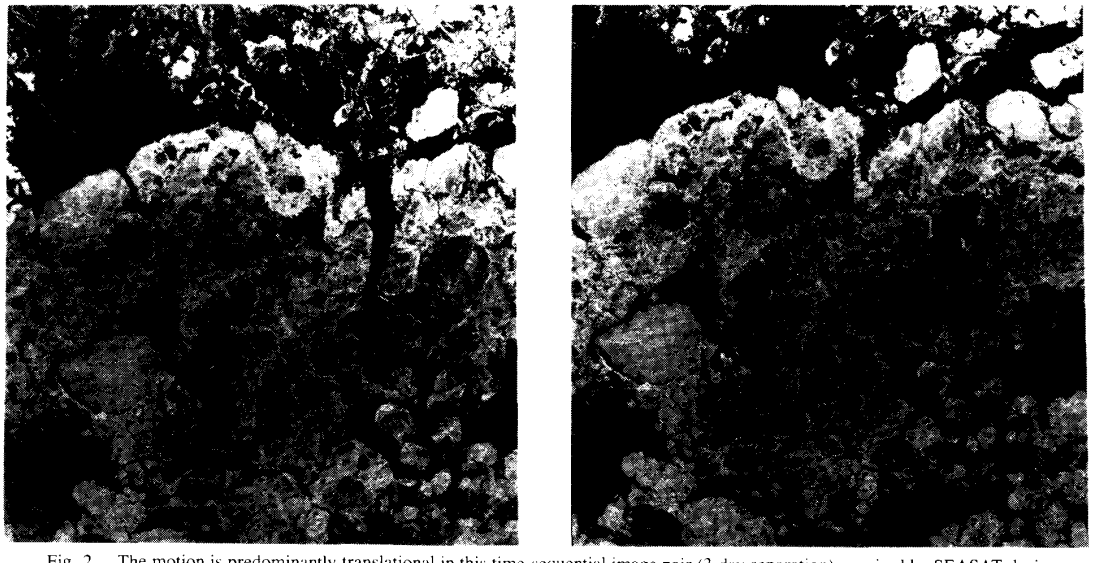

Fig. 2. The motion is predominantly translational in this time-sequential image pair (3-day separation) acquired by SEASAT during REVS 1409 and 1452, respectively.

In the central ice pack where the motion is predominantly translational with moderate rotation (Fig. 2), the area-based methods are fairly successful. However, in the ice margin (Fig. 3) where piecewise rotation and translation of the ice floes are routinely observed, these methods cannot measure these motion parameters with a high probability of success as required by the GPS.

An important requirement for an operational algorithm is to have the adaptivity and robustness to measure ice motion in both the context of the central ice pack as well as the ice margin. The algorithm described in this paper achieves this goal by using a hybrid approach which includes both feature-based and area-based tracking for construction of the ice-motion field from sequential images. This paper describes the automated motion tracking system which will be integrated into the Ice Processor of the GPS. The structure of the paper is as follows: An overview of the algorithm is given in Section II, followed by a description of the processor operations and interfaces in Section III. Section IV describes the ice-motion data product characteristics, followed by a discussion of the system in Section V.

II. Algorithm Overview

The primary objective of ice-motion analysis is to measure the mean deformation at the SAR image frame scales (roughly 100 km). Mean deformation can be estimated by measuring

Fig. 3. The ice floes in this time-sequntial pair (3-day separation, near the ice margin) have rotated as much as 40° relative to each other, thus requiring special processing during motion tracking.

displacements at a series of points around the boundary of an image frame and integrating the displacement around this boundary. Secondary objectives are to measure displacements on a grid (3 to 5 km spacing) to identify areas of ice which move as rigid pieces and to measure the deformations which occur between these rigid areas. To meet these objectives, the output of the motion tracker will provide sampling of the ice motion on a uniformly spaced grid.

A block diagram of the ice-motion tracking algorithm is shown in Fig. 4. The input to the tracker consists of geometrically and radiometrically corrected SAR images as well as the image-related parameter data. Geometric fidelity and the accurate earth location of these images are essential for the measurement of the absolute ice-motion and deformation field using sequential images. Absolute geolocation is required for accurate measurement of the mean deformation, whereas the local geometric fidelity determines the accuracy of the local shear and divergence measurements. In the geometric correction process each image is rectified and registered to a common Earth-fixed grid. The selected grid for the motion data is the SSMI grid, which is defined on a polar stereographic projection with the secant plane at 70°N. For the ERS-1 products generated at the ASF, the rectified images will have an expected absolute location uncertainty of less than 100 m and relative distortion of less than 0.1 percent relative to local variations from the assumed geoid [9], [10]. Relative radiometric calibration is important from the standpoint of image segmentation (extraction of image features), where consistency is required both across an image frame and from frame-to-frame to identify common features. For example, residual intensity gradients in an image due to a roll-angle offset in the antenna pattern correction will introduce errors in the feature extraction process (as discussed in the following sections). An overview of the function of each element in the block diagram

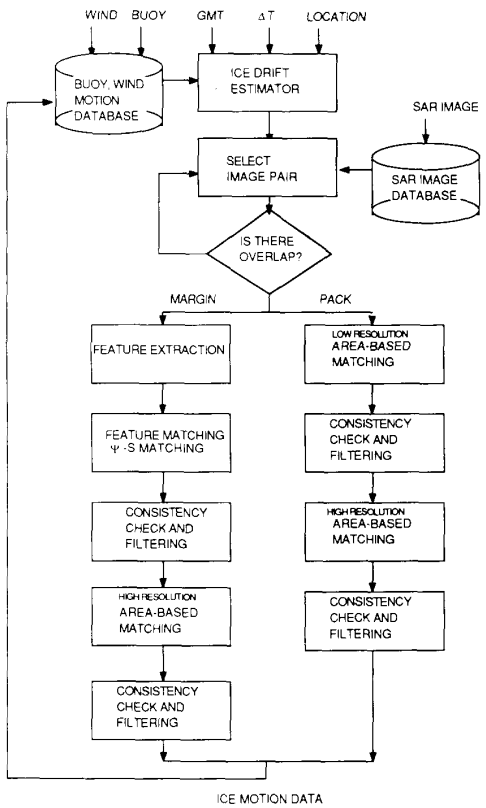

Fig. 4. Block diagram showing the flow of the combined feature-based and area-based motion-tracking algorithm.

is given in the balance of this section. Detailed descriptions of the image analysis techniques are given in [11].

A. Automated Image Pair Selection

The Lagrangian motion field is generated by first selecting a reference image that can be designated by the user or identified by geographic location. (The GPS will routinely generate ice-motion fields for selected areas of the Arctic—e.g., Beaufort Sea—without operator prompts.) A requirement for a fully automated system is the ability to select candidate image pairs without operator supervision. In our approach, the location of the corresponding ice field (containing approximately the same ice features) closest in time is determined by estimating the short-term (days) ice drift based on a linear model which relates the mean ice velocity $\boldsymbol{u}$ of an ice field within the SAR footprint to the geostrophic wind [12], [13], i.e.,

$$\boldsymbol{u} = A\boldsymbol{G}.$$

Here, $\boldsymbol{u}$, the ice velocity, and $\boldsymbol{G}$, the geostrophic wind, are vectors and are consequently treated as complex numbers. The term A is a complex multiplier, consisting of a scaling factor and an ageostrophic drift angle θ. The drift angle is measured clockwise from $\boldsymbol{G}$ to $\boldsymbol{u}$. This multiplier has a seasonal dependence and is characterized in the work of *Thorndike* and *Colony* [12]. The physical processes affecting the motion of ice are many; however, on the time scale of days, more than 70 percent of the variance of the ice motion is explained by the geostrophic wind alone, with minimal contributions from climatology. The time of separation between two sequential images collected by the polar orbiting SAR's are usually less than 20 days. Thus, a reduction in the search space for candidate image frames is afforded using this simplified wind-driven ice drift model.

The product of the mean velocity and the time separation between sequential images gives the estimated displacement of the ice field. This estimate then guides the search for the candidate image frames in the image database which have a high probability of containing the corresponding ice features. The model works well away from coastal influence and away from the marginal ice zone. Due to the stress gradients near the coastal regions and ice margin, more general motion models are required. In these regions, an exhaustive search for the corresponding image is performed in a neighborhood to locate the image pair. After a candidate image pair is found, a low-resolution implementation of the feature-tracking and area-tracking (described below) schemes is used to determine whether there are overlapping features. This step is iterated until an image pair with at least 50 percent over lap is found.

It should also be noted that the system also plans to ingest data from drifting buoys. If this capability is realized, then a more sophisticated ice-drift estimator which integrates wind and buoy measurements could be mechanized. Another potential dataset which could be used for ice-drift estimation is the results from the motion tracker itself. However the optimal combination of these measurements remains a research area.

B. Feature Extraction

After selection of the image pair, the algorithm proceeds to one of two steps, depending on whether they are located in the central ice pack, coastal zone, or ice margin. The rationale for this distinction is based on the characteristics of the motion field in these regions as they relate to the performance of the ice-motion tracking algorithm. In the central ice pack, the motion of the ice features are predominantly translational with moderate rotations, whereas the motion in the other two regions have large translational and rotational components requiring a different algorithm to optimize the construction of the ice-motion field.

Within the central ice pack, area-based matching techniques can be used for direct extraction of ice-motion data. It has been demonstrated [5]–[8] that the determination of the translational motion among image patches in time-sequential images is easily measured by two-dimensional cross correlation of the image patches where the spatial lag is given directly by the correlation peak. Therefore, for motion tracking in the ice pack the algorithm proceeds directly to the next stage, where a multistage area correlation strategy is used for image matching. However, this approach becomes unreliable if the large rotation of ice features is present.

In the ice margin, our approach to the tracking rotation is to use feature tracking for matching features that have translated and rotated. Preceding this tracking process is the extraction of distinct image features with a high probability of producing successful matches. In this case, the features used are region boundaries. Regions are defined as connected image areas that exhibit similar attributes in terms of pixel intensity and texture. The statistical textural attribute is a spatial variance measure extracted from a local sample window. To account for the combined variability due to speckle and texture, we adopt the normalized texture measure based on a multiplicative model of image mean, speckle noise, and texture [14], where

$$\left(\frac{\sigma_t}{\mu_t}\right)^2 = \frac{\left(\frac{\sigma_s}{\mu_s}\right)^2 - \left(\frac{\sigma_n}{\mu_n}\right)^2}{1 + \left(\frac{\sigma_n}{\mu_n}\right)^2}$$

where σ_t/μ_t, σ_s/μ_s, σ_n/μ_n are ratios of the standard of deviation to the mean of the image texture, detected image amplitude, and expected speckle noise, respectively. In the above equation, the speckle variance is removed from the square-root intensity image. The speckle noise ratio σ_n/μ_n is estimated using the number of looks associated with a SAR image. Removal of the speckle noise variance yields a more accurate measure of the sample texture.

Regions are formed by the automatic clustering of the image attributes. Clustering is essentially the partitioning of the attribute vectors in pattern space. An iterative global clustering procedure known as ISODATA [15] organizes the data into clusters, each of which is identified by a cluster centroid. A minimum distance classifier then assigns each attribute vector to its closest centroid, resulting in a mapping of each pixel into regions defined by the cluster centroids. An example of the region segmentation of an image is shown in Fig. 5. The segmented regions might be areas of different ice types or ice and open water. Separating the regions are boundaries which will be used in the next stage of the algorithm.

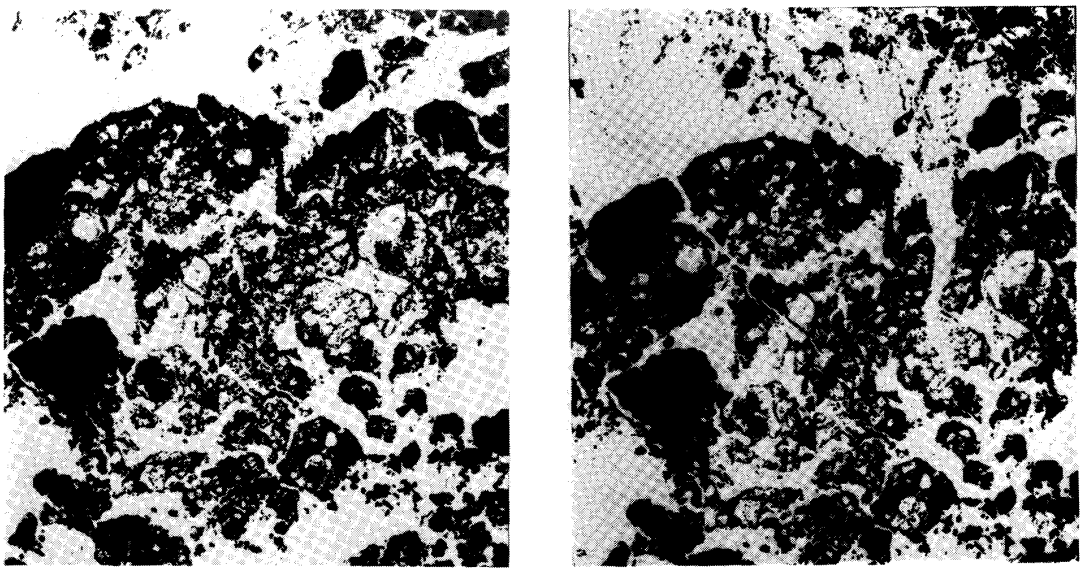

Fig. 5. Feature extraction: Results of clustering of image intensity and texture into two distinct regions. Original image pair is shown in Fig. 2.

The segmentation of statistically similar regions is an important first step when working with SAR image data because of the multiplicative characteristic of the speckle noise. The effect of this noise is a large variance in pixel values of homogeneous backscatter which can effectively mask real features or create false ones. The segmentation reduces the effect of the speckle by estimating the statistical behavior of this noise (Rayleigh distributed) and finding significant deviations in the image characteristics relative to the speckle that arise from variations in the target backscatter.

C. Feature Matching

Following image segmentation, the boundaries are vectorized to form one-dimensional data structures consisting of ordered pairs representing the boundary image coordinates. A transformation is applied to these coordinate pairs to generate a rotationally invariant curvilinear representation known as a (ψ, s) curve. Fig. 6 shows an example of a (ψ, s) curve. The angle ψ is made between a reference line and a tangent to the boundary of a shape. It is plotted as a function of s, the arc length of the boundary traversed [16]. This representation has the special advantage that any rotation of a region boundary is observed as a displacement of the (ψ, s) curve in the ordinate direction (i.e., a bias in ψ). The matching of the (ψ, s) curves from sequential images is accomplished by selecting a candidate (ψ, s) segment from one image (a segment being a short length of a (ψ, s) curve) and searching for the best match in the second image by successively shifting the segment along all features that have similar characteristics (i.e., similar image statistics on either side of the boundary). This process translates a computationally expensive two-dimensional correlation process into a very fast one-dimensional matching. The matching is done by the one-dimensional cross-correlation of the (ψ, s) segments, the similarity measure being the normalized correlation coefficient,

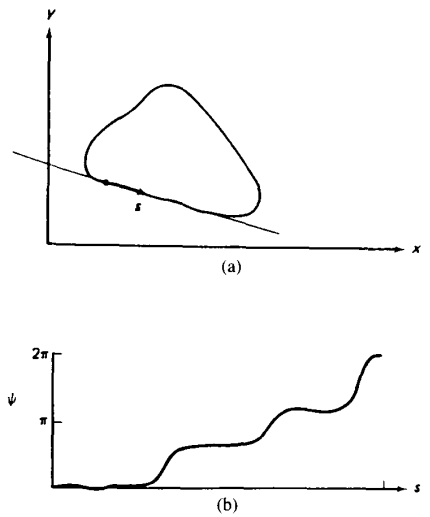

Fig. 6. ψ-s curve. (a) Triangular curve. (b) ψ-s representation of the curve. (reference [16]).

$$\rho(k) = \frac{\sum_{j=1}^{n} \psi_1(j)\psi_2(j-k) - \mu_1\mu_2}{\sigma_1\sigma_2}$$

where μ_i and σ_i are the mean and standard of deviation of the ith (ψ, s) curve, and N is the length of the segment. In addition to the correlation coefficient, the regression coefficient gives a measure of the scale difference between the corresponding curves and is used for filtering out bad matches when there is a large disparity in the scale of the two shapes.

The relative rotation θ of the features is obtained directly

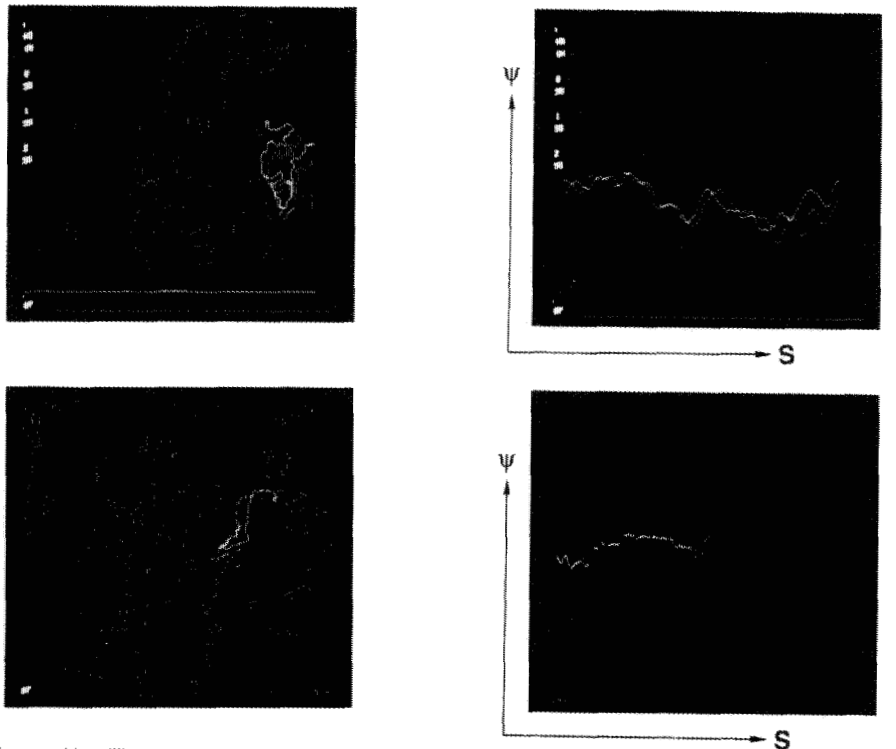

Fig. 7. ψ–s matching. The red and green boundaries are the region boundaries extracted from the image pair. (a) The location of a set of matched features (shown highlighted). (b) The corresponding features in the ψ–s representation. (c) The matches generated during this stage of the algorithm; the blue vectors connect the matched boundaries. Note that the matches are localized at the region boundaries.

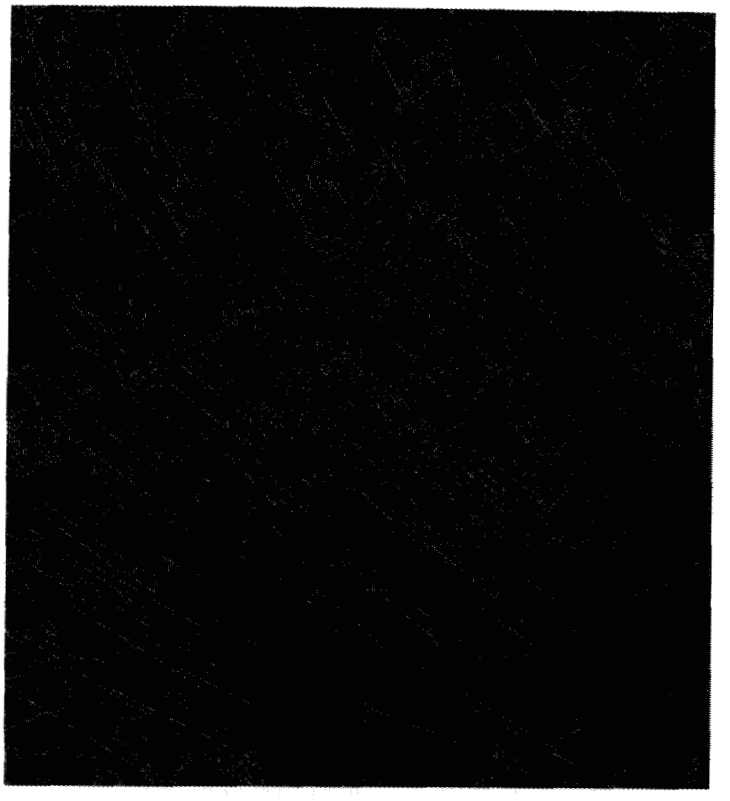

Fig. 8. The motion vectors generated from the matching of the region boundaries of the image pair shown in Fig. 1.

U-M-I

Due to a lack of contrast between text and background, this page did not reproduce well.

from

$$\theta = \mu_1 - \mu_2$$

while the mean displacement from the reference segment $\vec{d}$ is determined by

$$\vec{d} = \frac{1}{N}\sum_{i=1}^{N}(\vec{x}_i - \vec{y}_i)$$

where $\vec{x}$, $\vec{y}$ are the image coordinates of the matched boundary points. Thus the output from the feature matcher is both the rotational and translational motion of the segments as measured at the region boundaries. Fig. 7 shows an example of matched (ψ, s) segments. The vectors indicate the displacements of the matched segments or region boundaries. An example showing the full set of vectors that were generated during this stage (from the image pair in Fig. 1) is shown in Fig. 8.

D. Area-based Matching (Area Correlation)

The motion field generated by the feature matcher is localized at the region boundaries within the image frame and is in general a sparse nonuniform sampling of the ice motion. The feature matching is therefore followed by an area-based matching technique to sample the motion field on a uniformly spaced grid. It is based on two-dimensional cross correlation of the image intensities. In this case, the similarity measure is a two-dimensional normalized cross-correlation coefficient evaluated at candidate rotation angles θ:

$$\rho(m, n, \theta) = \frac{\sum_{i=1}^{N}\sum_{j=1}^{N} I_1(i, j; \theta)I_2(i-m, j-n) - \overline{I_1}\,\overline{I_2}}{\sigma_1\sigma_2}$$

where $\overline{I_1}, \overline{I_2}$, and σ_1, σ_2 are the image means and standard of deviations, respectively, and $N \times N$ is the size of the image patch. Here, I_1 is rotated by an small increment each time to generate the correlation surface with dependence in (m, n, θ).

The output of the feature matcher yields translation and rotation data at the region boundaries. It is used to initialize the area correlation matching, thus reducing the search space and increasing the algorithm throughput. The first step in the area correlation algorithm is to estimate the ice motion at the grid points. Candidate matches for a grid point are generated by selecting all matches within a pre-specified window centered at the point. This was determined to be better than using an interpolation scheme (for generating the motion estimate) where assumptions of smoothness and continuity cannot be supported, especially for discrete floes moving independently.

The second step is then to find the best match from the set of candidates. Effectively to locate the correct area, a three-dimensional search (translation and rotation of the image patch) is required to find the maxima in the correlation hypersurface, a computationally expensive process. To improve the efficiency in the correlation process, a technique for efficient registration of translated and rotated images using fast Fourier transforms [17] has been employed. Briefly, if $s_t(x, y)$ is a translated and rotated replica of $s_0(x, y)$, then according to the Fourier shift and rotation theorem their Fourier transforms are related by

$$S_t(\eta, \xi) = e^{-j(\eta x_0 + \xi y_0)}S_0(\eta\cos\theta_0 + \xi\sin\theta_0,\ -\eta\sin\theta_0 + \xi\cos\theta_0)$$

where (x_0, y_0) is the translation vector, and θ_0 is the rotation of the image patch. If the two-dimensional cross correlation is performed in the transform domain, the intermediate rotated image spectra can be created by nearest-neighbor resampling of the image spectrum, which has been oversampled in the forward transform. This technique eliminates the need for rotation in the image domain as well as all the associated forward transforms (after rotation in the image domain) into the Fourier domain. Fig. 9 shows examples of matched image patches with a fairly large angle of rotation between them.

For the case of the motion field in the ice pack where the motion is mostly translational, a two-stage area-matching algorithm is used. Image matching is done at a reduced resolution during the first stage. The approximate translation vectors are used to guide the image matching at the second higher resolution stage using the method described above.

E. Consistency Checks and Filtering of Bad Matches

As an operational system the ice-motion processor must meet minimum performance criteria in terms of the accuracy and consistency of the output motion fields. The design therefore includes a number of filtering process and verification checks based on correlation performance parameters, image statistics, and physical constraints of motion at different stages of the algorithm. The correlation performance parameters include the correlation peak, the regression coefficient, and, derived from the correlation surface, the correlation peak-to-background ratio. In order to filter out image patches that contain smooth areas (e.g., water, smooth new ice) from producing false matches, the statistical texture measure mentioned above is used. As far as motion consistency and constraints are concerned, the motion predicted at each grid point is compared with the motion of the neighboring points. The match is classified as false if there are no local matches which support the hypothesis that the motion measured at the point is correct.

F. Update Motion Field Database

The resultant motion field is populated by translation vectors and rotation data associated with the image patches. The spatial and temporal samples of the motion field are stored in a database which contains wind data as well as data gathered by the Arctic buoy array. As previously mentioned, this database will be maintained to initialize the motion estimator. These data could as well be used for the estimation of the mean deformation of the ice field in regions with sparsely spaced motion samples.

III. Processor Operations/Interfaces

This section presents an overview of the GPS architecture and operations, including its external interfaces and its interfaces to the Alaska SAR facility.

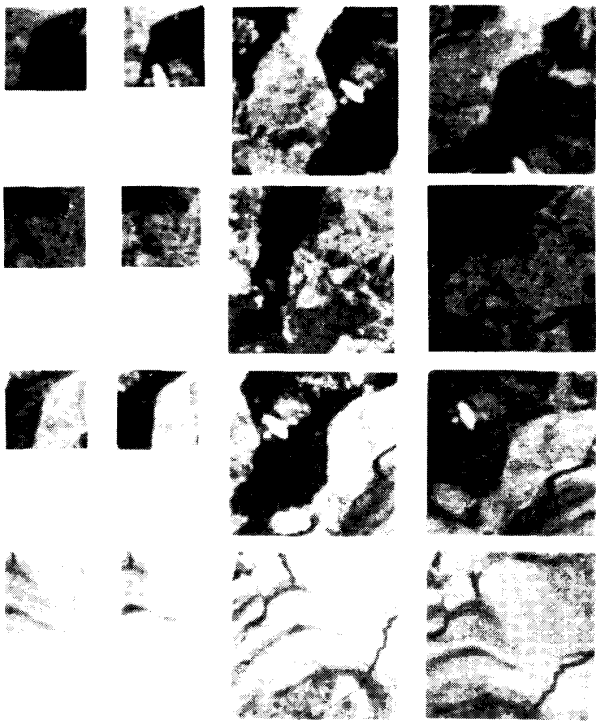

Fig. 9. Examples of matched image patches with fairly large relative rotation between the reference and target. (a) and (b) are 32×32 patches that were matched by the area correlation algorithm. (c) is a 64×64 image patch showing the image in the patch in the source image. (d) is a 64×64 image patch showing the same area in the target image.

A. ASF Interface

As mentioned previously, the ASF will consist of a Receiving Ground Subsystem (RGS), SAR Processing Subsystem (SPS), and an Archive and Operations Subsystem (AOS). The RGS will receive and record SAR signal data from the spaceborne radars. The SPS will process the radar signal data into both a high-resolution and low-resolution image. The low-resolution imagery is transferred to the AOS for archiving, cataloging, and dissimination. The AOS maintains an on-line archive of all low-resolution imagery acquired by the Alaska station. These on-line low-resolution image frames consist of 1×1 K pixels (1 Mbyte) covering a 100-Km area at 100-m pixel spacing. In the planned operational scenario, the GPS requests SAR image data from the AOS system and returns geophysical products to the AOS for archive and distribution. A block diagram of the two systems is shown in Fig. 1. Briefly, the AOS will provide to the GPS a daily summary report of all images processed in a 24-h period. Based on this report and the results of the ice-motion estimator, the GPS will then request detailed reports of images that are candidates for motion analysis. If the quality of the images is satisfactory, the image data will be copied from the AOS and fed into the motion-tracking algorithm. The standard motion products (described in the next section) will be returned to the AOS for archiving and distribution. User requests for motion products as well as other SAR image products are handled by the AOS.

B. External and Operator Interface

The GPS will have external communication links to NMC weather centers for accessing meterological data and buoy data. A menu-driven interface will be designed for interactive operator input and control of routine operations. In the event that the automated tracking software has determined that the process of image matching has progressed unsatisfactorily, the operator will be notified. An operator-assisted tiepointing package [18] is available for generating the motion field manually.

C. Hardware

The GPS is based on a high-performance workstation (SUN-4) with 32 MB of memory. It is augmented by a high-speed array processor capable of 15 million floating point operations per second. It will have the computational capability to handle motion product generation (10 per day) with excess capacity to handle proposed processing algorithms for ice-type classification and estimation of ocean wave spectra.

D. Database

Databases containing the ice-motion products, meterological data, and data gathered by the Arctic buoy array will be maintained by the GPS.

IV. Data Product Characteristics

Table I lists the data fields which will be included with each product. The standard input to the ice-motion tracker will be SAR images ($100 \times 100 -$ km coverage) with a spatial resolution of approximately 100 m, although the algorithm is not limited to images with these specifications. The output is a displacement field constructed from the time-sequential image pairs, the characteristics of which are outlined below.

A. Sample Density and Grid Description

The motion data will be sampled on a uniformly spaced grid with a sample spacing of 3 to 5 km. Each sample has a translation vector with an associated rotation angle. The rotation component, a consequence of the area-based matching, describes the rotation of the image patch. The geolocation of each earth-fixed grid point is defined on the SSMI projection. The absolute location accuracy of each grid point is approximately 100 m for the ERS-1 SAR. The rationale for selecting an earth-fixed grid is that it should provide a common reference for all motion data which is independent of the orientation of the sensor. This type of grid simplifies the tasks of image co-registration with correlative datasets, spatial mosaicking of motion data for large-scale modeling, as well as the spatio-temporal analysis of kinematics data.

B. Accuracy of Motion Data

The accuracy of the motion data is dependent on the invariance in the image structure and amount of deformation

TABLE I
ICE MOTION PRODUCT SPECIFICATIONS

Data Field	Description
Product Identifier	
Center Time - Image A	
Center Time - Image B	
Image ID - Image A	
Image ID - Image B	
Data Take ID - Image A	
Data Take ID - Image B	
Geographic Location: Image A	4 corners (latitude,longitude)
Geographic Location: Image B	4 corners (latitude,longitude)
Location: Image A	4 corners (grid coordinates)
Location: Image B	4 corners (grid coordinates)
Creation time	
Time of separation	Time separation of image pair
Software Version/Algorithm type	
Number of grid elements per line	
Number of grid points with matches	
Average displacement vector	
Grid Spacing	3 to 5km
Image Size - Image A	
Image Size - Image B	
Spare field (100 characters)	Comments
Wind Field	Used in motion estimation
Displacement vector, rotation angle, quality of match metric	For each grid point

within each area (image patch). Finer sampling of the local motion field can be obtained by selecting a smaller image patch. However, the amount of the image structure for area matching also decreases. Hence, the size of the image patch selected for matching purposes is a balance between these two factors. The patch sizes are between 3 to 5 km, less the spacing between the grid points. This is to avoid the correlation of the motion samples due to overlapping image features. Based on comparison of the tracker results with operator-selected tie-point measurements, the accuracy of the tracker is on the order of one-to-three resolution elements (100–300 m). A match quality metric, indicating the confidence of the match, will be provided with each data point. This measure is generated by the tracker using correlation performance parameters and consistency constraints. The intent of this metric is to allow users to do further filtering of the motion samples. For smooth areas like open water, where there are no "trackable" features, there will be no motion samples. As a result, the motion grid is not totally populated. An alternative is to estimate the motion at these points using adjacent data points. This would be feasible in the central ice pack where the local motion is usually smooth; however, in the ice margin the error introduced by interpolation would probably be quite high. The current design does not interpolate the motion field.

C. Examples and Results

Figs. 10 and 11 show examples of output products displayed vectors and rotation angles on uniformly spaced grids. Both of the sequential SAR image pairs were acquired by SEASAT over the Beaufort Sea during the fall of 1978. The pairs in each figure were imaged during REV 1409 and REV 1452, approximately a three-day separation in time. The displacement vectors and rotation angles were sampled on a 20×20 grid (5-km grid spacing). The vectors (for display purposes) are scaled such that their magnitude is less than the grid spacing. The motion in the first pair (Fig. 10) is predominantly translational with very little rotation. The second pair (Fig. 11) is located near the ice margin, and large rotations of the

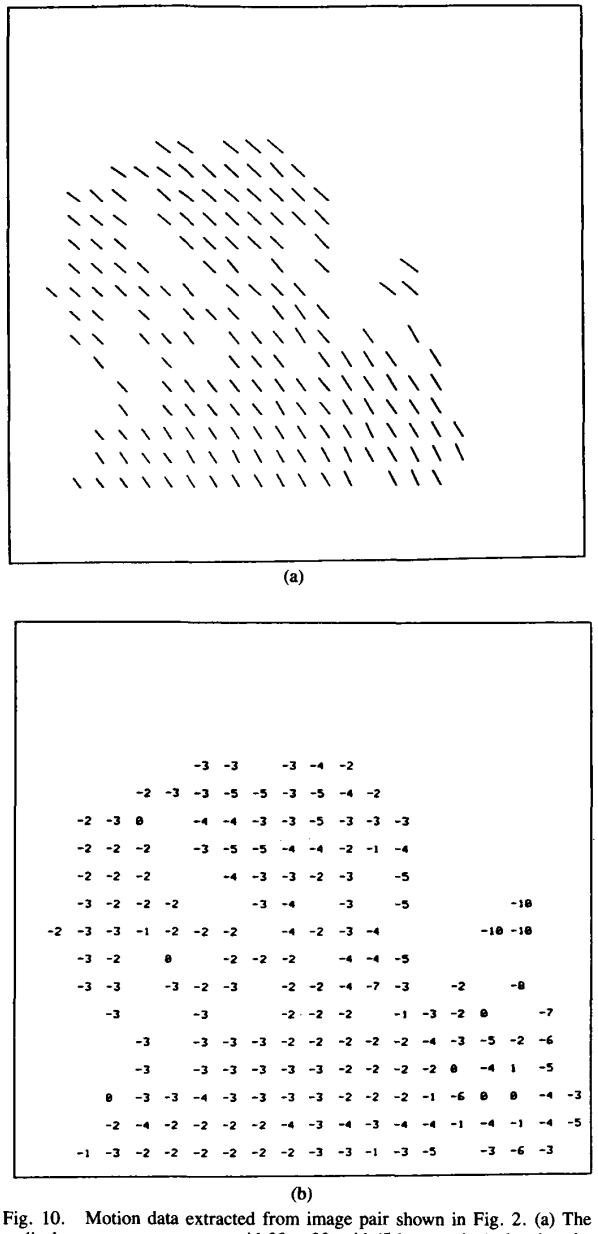

(a)

(b)

Fig. 10. Motion data extracted from image pair shown in Fig. 2. (a) The displacement vectors on a grid 20×20 grid (5-km spacing) showing the translation of the image patches over a 3-day period. (b) Rotation angles of the image patches on the same grid showing relatively little rotation.

ice floes can be observed. The ice floes act almost as discrete rigid bodies that have separate translational and rotational behavior. The empty grid points indicate that there are no corresponding features in the image pair (in this case, a feature in image 1 has moved out of the coverage of the image 2) or that the tracking algorithm did not generate a match due to a failure in meeting the match-quality conditions mentioned in Section II.

It should be noted that the wavelength of the SEASAT radar was 23 cm and that the European ERS-1 radar will be 5.6

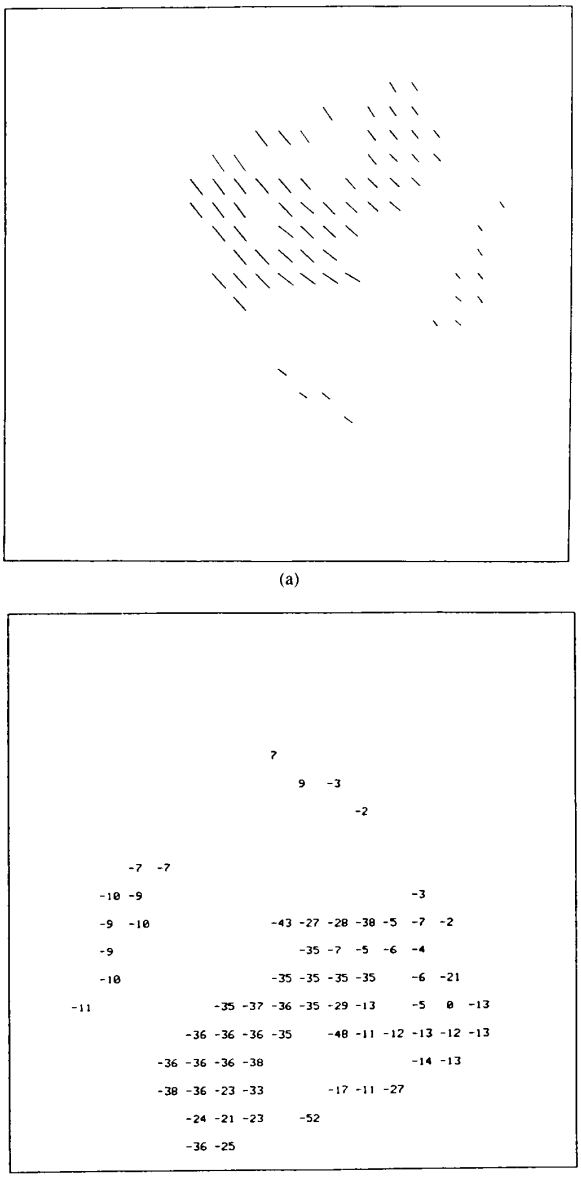

Fig. 11. Motion data extracted from the image pair shown in Fig. 3. (a) The displacement vectors on a grid 20 × 20 grid (5-km spacing) showing the translation of the image patches over a 3-day period. (b) Rotation angles of the image patches on the same grid showing large relative rotations.

cm, so the backscattering characteristics of the same ice floes and thereby the appearances of the images will be different. Presently, there does not exist a good dataset with *C*-band ice-motion pairs which provide the expected coverage, resolution, and image quality of the ERS-1 SAR. As a consequence, the motion tracker can only be directly verified using SEASAT images. Elements of the motion algorithm such as the feature extraction algorithm have been tested with *C*-band radar images from the NASA DC-8 program with consistent results. The implementation plan includes an initial post-launch phase that will be a period for the refinement and adjustment of the motion-tracking parameters for performance optimization.

V. Summary

In addition to all-weather and day–night coverage, the SAR provides a sampling of sea-ice motion over large spatial and temporal scales. An ice kinematic dataset generated by using sequential imagery will serve as input to large-scale and small-scale ice-motion models for aiding in the understanding of ice processes, as well as input to an applications area such as the monitoring of sea ice for navigational and commercial purposes.

An operational system for the extraction of ice-motion data from SAR images will be installed at the Alaska SAR Facility for the routine generation of these kinematic datasets. The system and the automated algorithm which use a hybrid approach of feature-based and area-based matching for determining the motion field of the ice features are described in this paper. The ice-motion tracker has been tested with *L*-band SEASAT data, and the feature extraction algorithm with *C*-band aircraft data. Refinement of the algorithm will continue into the post-launch checkout period when ERS-1 data is available. Since the system is based on commercially available hardware and software, the system could easily be duplicated at remote user sites. Additionally, the motion-tracking algorithm can easily be modified for analysis of ice motion from sequential images acquired by other sensors.

Acknowledgment

The authors wish to thank R. Fätland for contributions to the software development effort and A. Pang and J. Weirick for data processing support and F. Leberl of Vexcel for insightful suggestion in the algorithm development.

References

[1] F. Carsey and B. Holt, "Beaufort-Chukchi ice margin data from Seasat: Ice motion," *J. Geophys. Res.*, vol. 92, pp. 7163–7172, 1987.

[2] R. T. Hall and D. A. Rothrock, "Sea-ice displacements from SEASAT synthetic aperture radar," *J. Geophys. Res.*, vol. 86, pp. 11078–11082, 1981.

[3] F. Leberl, J. Raggam, C. Elachi, and W. J. Campbell, "Sea-ice measurements from Seasat SAR images," *J. Geophys. Res.*, vol. 88, pp. 1915–1928, 1983.

[4] J. C. Curlander, B. Holt, and K. J. Hussey, "Determination of sea-ice motion using digital SAR imagery," *IEEE J. Oceanic Eng.*, vol. OE-10, pp. 358–367, Oct. 1985.

[5] R. M. Ninnis, W. J. Emery, and M. J. Collins, "Automated extraction of pack ice motion from advanced very high resolution radiometer imagery," *J. Geophys. Res.*, vol. 91, pp. 10725–10734, 1986.

[6] M. Fily and D. A. Rothrock, "Sea-ice tracking by nested correlations," *IEEE Trans. Geosci. Remote Sensing*, vol. GE-25, pp. 570–580, Sept. 1987.

[7] J. F. Vesecky, R. Samadani, M. P. Smith, J. M. Daida, and R. N. Bracewell, "Observation of sea-ice dynamics using synthetic aperture radar images: Automated analysis," *IEEE Trans. Geosci. Remote Sensing*, vol. 26, pp. 38–48, Jan. 1988.

[8] M. J. Collins and W. J. Emery, "A computational method for estimating sea-ice motion in sequential Seasat synthetic aperture radar imagery by matched filtering," *J. Geophys. Res.*, vol. 93, pp. 9241–9251, 1988.

[9] J. C. Curlander, "Location of spaceborne SAR imagery," *IEEE Trans. Geosci. Remote Sensing*, vol. 20, pp. 359–369, July 1982.

[10] J. C. Curlander, R. Kwok, and S. S. Pang, "A post-processing system for automated rectification and registration of spaceborne SAR imagery," *Int. J. Remote Sensing*, vol. 8, pp. 621–638, 1987.

[11] R. Kwok and R. McConnell, "Object-tracking in a two-dimensional field,," to be published.
[12] A. S. Thorndike and R. Colony, "Sea-ice motion in response to geostrophic winds," *J. Geophys. Res.*, vol. 87, pp. 5845-5852, 1982.
[13] R. Colony and A. S. Thorndike, "An estimate of the mean field of Arctic sea ice motion," *J. Geophys. Res.*, vol. 89, pp. 10623-10629, 1984.
[14] F. T. Ulaby, F. Kouyate, B. Brisco, and T. H. L. Williams, "Textural information in SAR images," *IEEE Trans. Geosci. Remote Sensing*, vol. GE-24, pp. 234-245, Mar. 1986.
[15] G. H. Ball and D. J. Hall, "Isodata: A novel method of data analysis and pattern classification," NTIS, Alexandria, VA, NTIS Rep. AD699616, 1965.
[16] D. H. Ballard and C. M. Brown, *Computer Vision*. Englewood Cliffs, NJ: Prentice-Hall, 1982.
[17] E. De Castro and C. Morandi, "Registration of translated and rotated images using finite Fourier transforms," *IEEE Trans. Pattern Anal. Machine Intell.*, vol. 6, pp. 700-703, 1987.
[18] M. Lee, "Sea-ice analysis software—ICEMAN," in *Proc. IGARSS* (Edinburgh, Scotland), 1988, pp. 1713-1716.

★

Ronald Kwok (S'82-M'84) received the B.Sc. (summa cum laude) degree from Texas A&M University, College Station, in 1976, and the Ph.D. degree from Duke University, Durham, NC, in 1980. He was a Postdoctoral Fellow at the University of British Columbia, Vancouver, BC, Can., in 1981.

From 1981-1985 he was with MDA in Richmond, BC, where he worked on algorithms for Landsat and Radarsat ground data systems. In 1985 he joined the Radar Science and Engineering Division at the Jet Propulsion Laboratory in Pasadena, CA, where he developed techniques for the analysis of SAR imagery and served in a radar system engineering capacity on the Magellan and Alaska SAR facility projects. He is currently Group Leader in the SAR Systems Development and Processing Group, responsible for research and development of post-processing and analysis techniques for SAR image data.

Dr. Kwok is a member of Tau Beta Pi, Phi Kappa Phi, and Eta Kappa Nu.

★

John C. Curlander was born in Baltimore, MD, in 1954. He received the B.S.E.E. (Hons.) and M.S.E.E. degrees in electrical engineering from the University of Colorado, Boulder, in 1976 and 1977, respectively, and the Ph.D. degree from the University of Southern California, Los Angeles, in 1985.

From 1977 to 1978 he was with the Institute for Telecommunication Sciences in Boulder, where he worked in the area of high-speed digital communication systems. In 1980 he joined the Radar Signal Processing Research Group at the Jet Propulsion Laboratory in Pasadena, CA. There his work has centered on research in the area of synthetic aperture radar digital image processing. He is currently involved in systems engineering for the Shuttle Imaging Radar project and Venus Radar Mapper and is Group Supervisor of the Radar Systems Development and Processing Group, responsible for SAR signal-processing research and development of ground-based processing systems.

Dr. Curlander is a member of Tau Beta Pi and Eta Kappa Nu. He has received NASA Achievement Awards for his contributions to the development of the SEASAT SAR Digital Processor and the Shuttle Imaging Radar projects, the 1984 IEEE Browder J. Thompson Prize Paper Award for his paper, "Location of Spaceborne SAR Imagery," the IEEE Geoscience and Remote Sensing Society's Centennial Award for Young Engineers, and the 1988 NASA Exceptional Service Medal for his work in SAR processing and post-processing techniques.

★

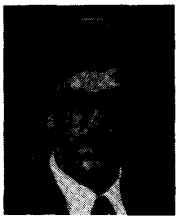

Ross McConnell was born in Denver, CO, in 1958. He received the B.A. degree from Williams College, Williamstown, MA, in 1981, and the M.S. degree from the University of Denver in 1985.

Since 1985 he has been at the Vexcel Corporation, Boulder, where his activities have included development of algorithms for tracking ice floes in SAR images and for registering opposite-side SAR imagery.

★

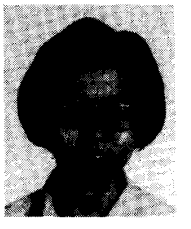

Shirley S. Pang received the B.A. degree in mathematics from Douglass College, New Brunswick, NJ, and the M.S. degree in computer science from the University of Hawaii, Honolulu.

She joined the Jet Propulsion Laboratory in Pasadena, CA, in 1973 and has participated in the software design and development for various interplanetary flight projects and ground-processing systems. She is currently involved in the software development for the Alaska SAR Facility Geophysical Processor System (GPS) and Archive and Operations System (AOS), as well as the Shuttle Imaging Radar Project.

Ms. Pang is the recipient of five NASA Group Achievement awards for her contributions to the Viking, Voyager, and Infrared Astronomical Satellite (IRAS) projects, and the Interim Digital Processor (IDP) and the Shuttle Imaging Radar B (SIR-B) processor.